

## SUPPLEMENTARY TEXT and FIGURES

### SUPPLEMENTARY TEXT

#### S1. Spatial sampling requirements at the detector plane

To complement the arguments made in the Appendix of the main text, the required pixel size ( $\Delta x_D$ ) at the detector plane for accurate sampling of the cell holograms can be obtained by considering the spatial frequency bandwidth of each cell hologram. Using Eqs. 3-4 of the Appendix for a narrow enough  $p(-x_D/M, -y_D/M)$ , based on the Nyquist sampling theorem<sup>36</sup>, one can derive the following spatial sampling requirement at the detector (assuming  $n=1$ ; cell width  $L_C$ ; cell hologram width  $L_H$ ):

$$\frac{1}{\Delta x_D} \geq \frac{(L_C+L_H)}{\lambda_0 \Delta z} = \frac{(L_C+L_H)z_1}{\lambda_0 (z_1+z_2)z_2} \quad \text{or} \quad \Delta x_D \leq \frac{\lambda_0 z_2}{(L_C+L_H)} \cdot F \quad (\text{S1})$$

According to Eqs. 3-4 of the Appendix, each scattering point within the cell body diffracts coherently with respect to the background light over a distance of  $\Delta z = (z_1 + z_2)z_2/z_1$  which validates the applicability of Eq. S1 to our results even with an *incoherent source emanating from a large aperture*.

For  $M \gg 1$ ,  $F = \frac{z_1+z_2}{z_1}$  approaches 1 such that Eq. S1 can be simplified as:  $\Delta x_D \leq \frac{\lambda_0 z_2}{(L_C+L_H)}$ . However, for  $M \ll 1$ ,  $F$  approaches  $1/M$  such that the pixel size requirement of Eq. S1 becomes much relaxed.

Therefore the analysis presented in Eq. S1 points to an important trade-off: To be able to use incoherent light through a large aperture ( $D$ ) and still claim a decent spatial resolution based on lensfree holography, one would need a large  $M$  such that the smoothing affect of  $D/M$  on the cell image becomes negligible when compared to the target spatial resolution. However there is a price paid for this (described by Eq. S1), i.e., a smaller pixel size is now required when compared to  $M \ll 1$  operating at a similar  $z_2$  value. In conventional digital in-line holography systems, the pixel size requirement at the detector end is relaxed approximately by a factor of  $F$ , which is referred to as the "*fringe magnification factor*" as also discussed in the previous section. With a large fringe magnification factor, the limiting effect of the pixel size on the extent of the hologram ( $L_H$ ) is reduced, such that a much better resolution than the pixel size can be claimed. The down side of a large  $F$  is that the available field-of-view for a given detector array is also scaled down approximately by  $F^2$ , reducing the overall field-of-view of the system.  *$M \gg 1$  choice implies a fringe magnification of unity ( $F \approx 1$ ), which puts the burden on a tighter pixel size, while the requirements on the source spatial*

*coherence, mechanical stability, aperture size and cost are much relaxed together with a significant gain in the imaging field-of-view and light throughput.* As highlighted in the Results and Discussion Sections, despite this tight pixel size requirement, a sub-pixel resolution can still be claimed in the presented lensless approach through iterative holographic reconstruction.

## **S2. Space-bandwidth product and lensfree cell holography**

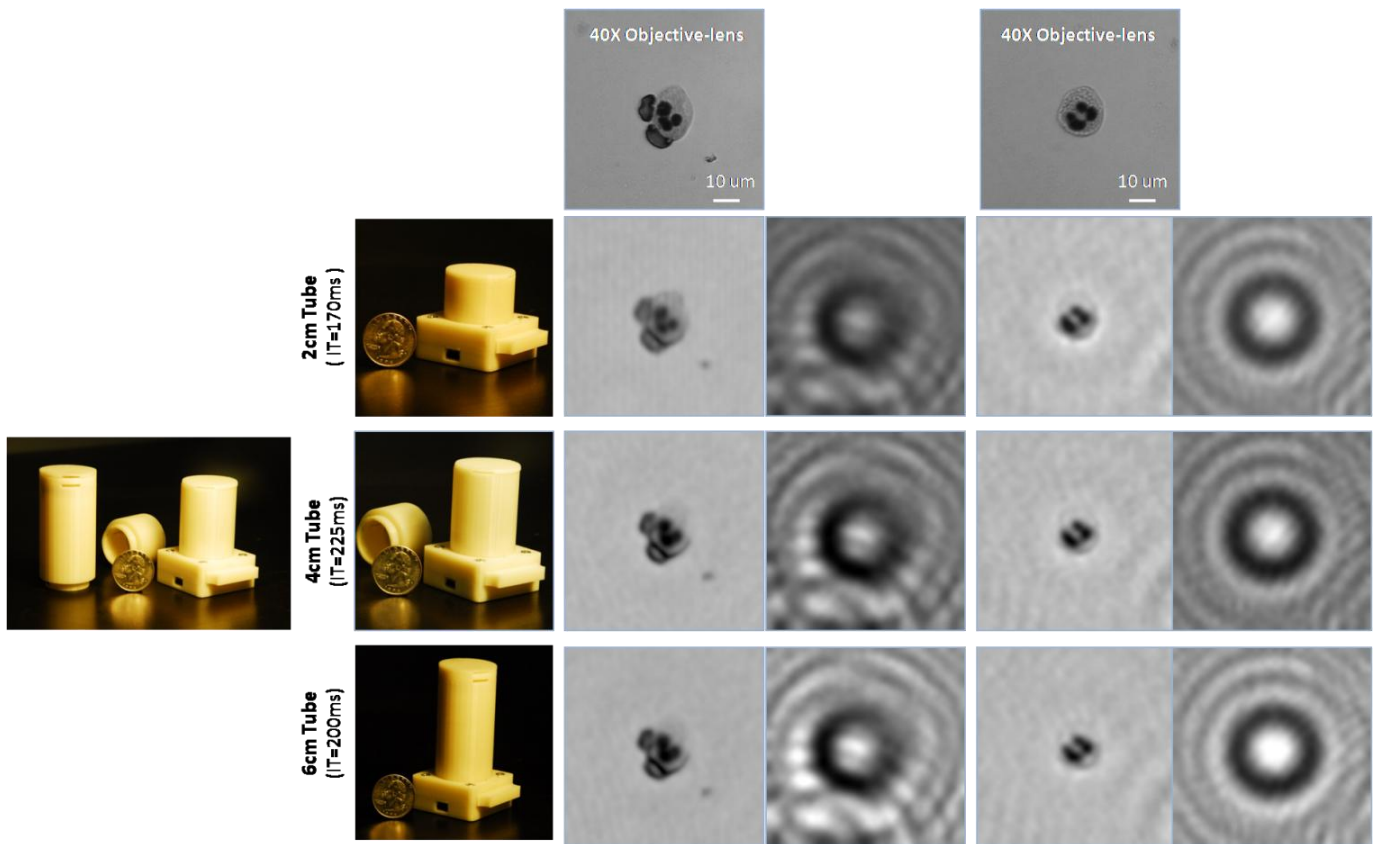
To better understand the space-bandwidth product requirements at the detector end for lensfree cell holography, let us denote the sensor width as  $W_D$ . Therefore, the space-bandwidth product (SB) of the detector can be written as  $SB_D = \frac{W_D}{\Delta x_D}$ . During coherent diffraction process, space-bandwidth product of a wave does not change; however, the space-frequency map (i.e., its Wigner distribution<sup>37</sup>) gets distorted by a lateral shear without changing its area. This linear shear (which is proportional to  $\lambda_0 \Delta z \Delta f$  in our case, where  $\Delta f$  is the spatial bandwidth of the cell's field transmission) also increases the required space-bandwidth product at the detector end. Therefore, in the presented incoherent holographic imaging approach, as a result of lensfree operation a space-bandwidth penalty of approximately  $\lambda_0 \Delta z \Delta f^2$  is to be paid.<sup>37-38</sup> Note that for  $M \gg 1$  operation, according to Eqs. 3-4 of the Appendix, despite the incoherent source, each cell is coherently diffracting over an effective distance of  $\Delta z$  before being sampled by the detector. Therefore, the SB product that is required at the detector array to sample each cell hologram in our case can be approximated as  $SB_C + \lambda_0 \Delta z \Delta f^2$  where  $SB_C = L_C \cdot \Delta f$  is the original space-bandwidth product of the cell. As a result of this, the penalty of incoherent source and free space propagation is an increased SB product at the detector by  $\lambda_0 \Delta z \Delta f^2$ . Once again, a weakly scattering cell is assumed here where otherwise the intensity detection at the sensor array would have added an additional factor of 2 for the required space-bandwidth product since the self-interference terms will now start dominating the detected quantities.

This SB penalty gets smaller by choosing a small  $z_2$  value, which is an argument in favor of  $M \gg 1$ . However, one should be careful with this statement: in the far-field region, where  $M \gg 1$  is no longer valid, because of the spatial Fourier transformation through free space, the space-frequency map of a wave gets flipped by  $90^\circ$ , which implies that a space-bandwidth product of  $L_C \cdot \Delta f$  would be sufficient for the detector end, which this time detects the Fourier transform intensities. Another way

of stating this conclusion is that Fresnel diffraction requires a significant penalty for space-bandwidth product at the detector end, whereas the Fourier transform plane (i.e., Fraunhofer region) is still as efficient as the original image in terms of the space-bandwidth product requirement for detection. Thus, *the price that is paid for a lensless system is an increased space-bandwidth product when compared to Fourier or image plane (i.e., lens-) based detection.* In the case of  $M \ll 1$ , of course, the imaging field-of-view will be significantly reduced when compared to  $M \gg 1$  case, as well as the individual holographic signatures of the cells will be lost, which can be considered as a loss for diagnostic purposes as the 2D texture of holographic cell signatures is also valuable for cytometry applications.<sup>22</sup>

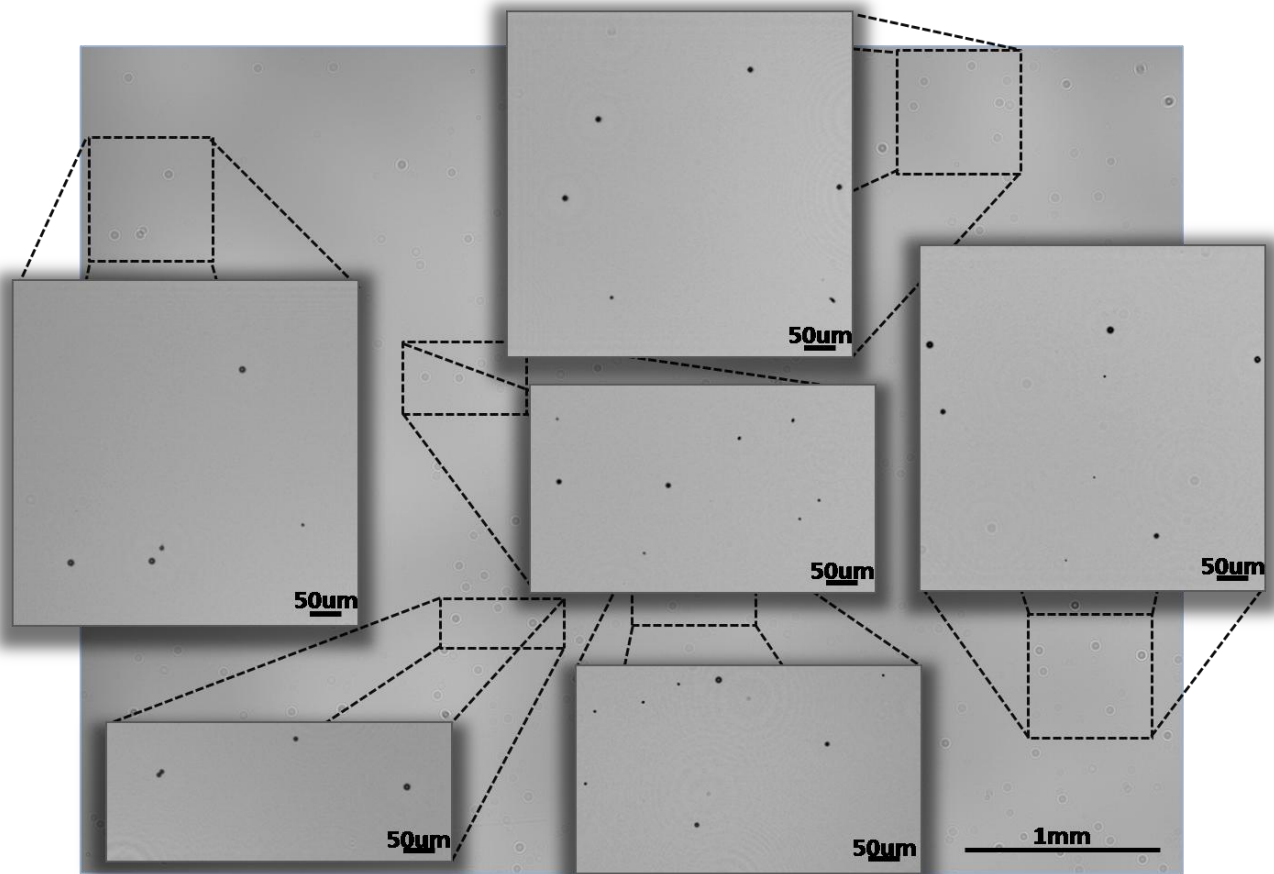
## SUPPLEMENTARY FIGURES

### SUPPLEMENTARY FIGURE 1



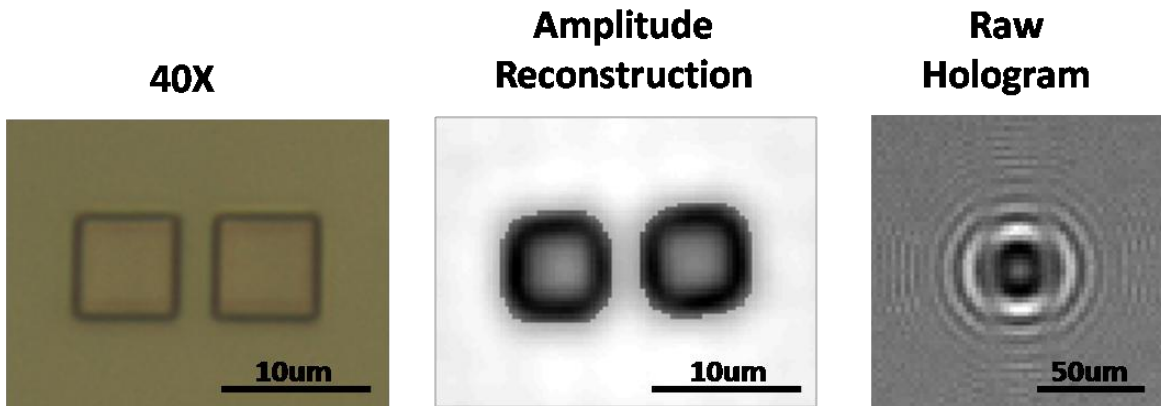
**Supplementary Figure 1.** Same as Fig. 3 of the main text, except for different tube designs. In the main text, Fig. 3 illustrates the performance of the 4 cm tube design (shown in Fig. 1(a)), whereas here we compare the imaging performances of 2, 4 and 6 cm tubes against a 40X objective-lens (NA=0.6). IT: integration time of the acquired raw lensfree hologram, shown to the right of each reconstructed image.

## SUPPLEMENTARY FIGURE 2



**Supplementary Figure 2.** Full field-of-view reconstructed image of a sample that is composed of 3, 7 and 10  $\mu\text{m}$  polystyrene particles is illustrated. The raw holographic image is captured using the lensfree microscope of Fig. 1(a).

### SUPPLEMENTARY FIGURE 3



**Supplementary Figure 3.** A test feature is imaged using the lensless holographic microscope with an LED at 591nm ( $D=50\ \mu\text{m}$ ,  $z_1\sim 3\text{cm}$  and  $z_2\sim 0.7\text{mm}$ ) and is compared against a 40X objective-lens ( $\text{NA}=0.6$ ) image. The gap between the squares is estimated as  $1.94\ \mu\text{m}$  (FWHM) from the reconstructed image, which matches very well with the gap estimate from the 40X image ( $1.95\ \mu\text{m}$  FWHM). Integration time for the raw hologram:  $<150\ \text{ms}$ .